Title: *Antennapedia* regulates metallic silver wing scale development and cell shape in *Bicyclus anynana* butterflies

Authors: Anupama Prakash[1*], Cédric Finet[2], Vinodkumar Saranathan[2], Antónia Monteiro[1,2*]

Affiliations:

[1] Department of Biological Sciences, National University of Singapore, Singapore.

[2] Division of Science, Yale-NUS College, National University of Singapore, Singapore.

*Correspondence to: anupama@u.nus.edu or antonia.monteiro@nus.edu.sg

Abstract: Butterfly wing scale cells can develop very intricate cuticular nanostructures that interact with light to produce structural colors such as silver, but the genetic basis of such nanostructures is mostly unexplored. Here, we address the genetic basis of metallic silver scale development by leveraging existing crispants in the butterfly *Bicyclus anynana*, where knockouts of five genes – *apterous A*, *Ultrabithorax*, *doublesex*, *Antennapedia* and *optix* – either led to ectopic gains or losses of silver scales. Most wildtype silver scales had low amounts of pigmentation and exhibited a common ultrastructural modification for metallic broadband reflectance, i.e., an undulatory air layer enclosed by an upper and lower lamina. Crispant brown scales differed from wildtype silver scales via the loss of the continuous upper lamina, increased lower lamina thickness, and increased pigmentation. The reverse was seen when brown scales became silver. On the forewings, we identified *Antennapedia* as a high-level selector gene, acting through *doublesex* to induce silver scale development in males and having a novel, post-embryonic role in the determination of ridge and crossrib orientation and overall scale cell shape in both sexes. We propose that *apterous A* and *Ultrabithorax* repress *Antennapedia* on the dorsal forewings and ventral hindwings, respectively, thereby repressing silver scale development, whereas *apterous A* activates the same GRN on the dorsal hindwings, promoting silver scales.

Introduction

Silver or gold colors in insect cuticles (1–3), fish scales (4), and the eyes of cephalopods (1, 4–6) are all examples of naturally occurring broadband structural coloration. These colors/structures serve multiple ecological functions such as in promoting vision, in serving as inter- or intra-specific signals, or in thermoregulation (5, 7–12) and arise from the interaction of light with specific classes of broadband reflectors found in the animal integument (13–15).

Broadband metallic reflectors are highly reflective across a broad range of wavelengths and are often thick structures. The most common type of reflector involves thin film or multi-layer interference reflectors made of alternating materials with different refractive indices and varying thicknesses (1, 16). Chirped multilayer reflectors, which vary the optical thickness of each layer systematically with depth, are found in the exocuticle of gold beetles (16, 17) or the endocuticle of pupal cases in some butterflies (3, 18, 19). When the optical thickness of each layer changes randomly with depth, like in the alternating layers of guanine crystals and cytoplasm in fish scales, they form chaotic multilayer stacks that have silver reflectances (6, 20). Due to the small difference in refractive indices of biological materials, broadband multilayer reflectors with high reflectivity usually require a minimum of 10-20 alternating layers of high- and low-refractive index materials, leading to very thick (tens of microns) multilayer reflectors (19).

In contrast, broadband metallic reflectors found in lepidopteran wing scales are anatomically constrained by the thickness of the scales. These metallic reflectors are ultra-thin, with an overall thickness of a few microns (10, 21–24). It has been suggested that broadband reflectance is achieved by additive color mixing that occurs due to local spatial variation or disorder in the scale ultrastructure (10, 21, 23–25). An essential modification of the basic scale Bauplan to produce such broadband reflectors appears to be the consistent presence of a contiguous upper lamina that closes the normally "open" windows seen in a typical scale (10, 21, 24, 26). This creates an undulatory air layer sandwiched by the lower and upper laminas whose thicknesses also spatially vary. The broadband metallic reflectors, seen in fossil (23, 27) and extant moths (22), and more basal springtails (28), however, utilize thin film interference from a single chitin layer, resulting from fused scales. The lower lamina of an open-type plan scale in butterflies is often also tuned to produce broadband colors (29, 30). Therefore, both the necessity and the optical role of the upper lamina and the air layer in broadband color generation are enigmatic.

The production of metallic broadband reflectors may also depend on the presence or absence of pigments embedded in the scale cuticle. For instance, the brown ground scales in *Hypolimnas salmacis* or the yellow scales in *Heliconius* butterflies have a closed upper lamina, but these scales do not exhibit broadband reflectance due to the high concentration of pigments (31, 32).

63 Furthermore, the retention of an upper lamina in a *yellow* mutant in *Bicyclus anynana* butterflies
64 (33), does not lead to metallic scales, either due to the presence of pigments or incorrect thicknesses
65 of both the laminas and air gap in these scales. These examples suggest that the GRN that creates
66 a metallic scale type must involve regulation of both scale ultrastructure and pigmentation. Yet,
67 despite numerous studies having addressed the structural origins of biological broadband
68 reflections across arthropods (3, 10, 19, 21, 23, 25) and its evolution within butterflies (24), the
69 optical basis, the genetic circuits, and developmental mechanisms that create these broadband
70 metallic reflectors remain sparse and unexplored.
71
72 We have begun to explore the genetic basis of silver scale development with a series of CRISPR
73 experiments performed in the nymphalid butterfly *B. anynana*. This species exhibits different types
74 of broadband reflecting metallic scales on both fore- and hindwings (34). These scales are usually
75 associated with the sex pheromone producing regions in males (the androconia), except for the
76 coupling scales near the base of the wings that are present in both sexes. Previously, the knockout
77 of five genes including *apterous A* (*apA*) (35), *Ultrabithorax* (*Ubx*) (36), *doublesex* (*dsx*) (34),
78 *Antennapedia* (*Antp*) (36) and *optix* (37) led to phenotypic effects on metallic scale development
79 in *B. anynana* (Fig 1A). Some knockouts produced ectopic brown to silver scale transformations
80 (*Ubx* and *apA*), whereas other knockouts led to the loss of silver broadband reflection and turned
81 the scales brown (*Antp*, *dsx*, *apA* and *optix*) (Fig 1A). These modified scales provide a great
82 opportunity to investigate the structural basis of the different metallic colors in *B. anynana* scales
83 and understand the roles of these five genes in creating broadband reflectors in lepidopterans.
84
85 Here, we asked whether these genes modified different structural and pigmentary aspects and
86 components of the scale to create a silver color, and vice versa, when silver scales became brown.
87 We also investigated whether transformations of different structures and levels of pigmentation
88 within a scale, with the manipulation of each gene in isolation, is complete or gradual. We
89 hypothesized that more up-stream genes regulating the silver scale GRN will produce more
90 complete and extreme transformations of the scales, making them resemble a wildtype silver scale
91 (or a brown scale) more closely. We also posited that each gene may be involved in regulating a
92 subset of the characteristics of silver or brown scales, or, alternatively, may be regulating all of its
93 distinctive traits but only partially.

To answer these questions, we used light, conventional and focused ion beam (FIB) scanning electron microscopy (SEM), UV-VIS-NIR microspectrophotometry, and systematic optical modeling, to understand different aspects of the wildtype (WT) and transformed scales. We show that the variable air gap thickness in silver scales is an important determinant of the broadband reflectance. Transformation of silver to brown scales is accompanied by the loss of the contiguous upper lamina, increases in lower lamina thickness and gains in pigmentation. The opposite occurs when brown scales become silver scales. In addition, we identify *Antp* as a top regulator of the silver scale GRN along with a novel role of this gene in determining scale shape.

Results

Ultrastructural and optical origin of broadband silver reflections in *Bicyclus anynana* butterflies

We first investigated how the silver color is produced in five types of silver scales present on the wings of *B. anynana* using light reflection and absorbance measures, as well as SEM (Fig. 1B-F). On the ventral forewing, we focused on the silver and the gland scales on the androconial patch of males (Fig 1A, WT-FW arrows). On the dorsal hindwing, we sampled the silver and grey-silver scales near the androconial patches of males. Finally, we sampled coupling scales near the base of the dorsal hindwing in females (Fig 1A, WT-HW arrows). All silver scales generally feature rounded edges. The coupling scales, however, have a characteristic trowel-head shape (Fig 1F, F′), and their ridges are oriented at an angle to the proximo-distal axis of the scale as compared to the parallel arrangement of ridges in most other scale types. The abwing and adwing surfaces of the scales exhibited an oil-slick like multi-hued appearance, typical of a thin film with varying thickness (Fig 1B-F). The reflectance spectra of all silver scales exhibited broadband reflectance, with higher intensities from the adwing surface (Fig 1B‴-F‴). Pigmentation levels were low in all scales, as measured from low light absorbance (Fig 1B⁗- F⁗), with the exception of the grey-silver scales which absorbed more light, indicating the presence of pigments. All silver scales exhibited a closed upper lamina (Fig 1B″-F″). The different silver scale types exhibited varying levels of perforations in the total area of upper lamina (Fig 1H, Supplementary Table S5 – source data): from ~0% (fore- and hindwing silver scales) and 2.35% (hindwing coupling scales), to 5.4% open (hindwing grey-silver scales) (Supplementary Tables S1,2). This correlation between the

integrity of the upper lamina coverage to the production of broadband reflectance affirms the important role attributed to the upper lamina and/or the enclosed air layer.

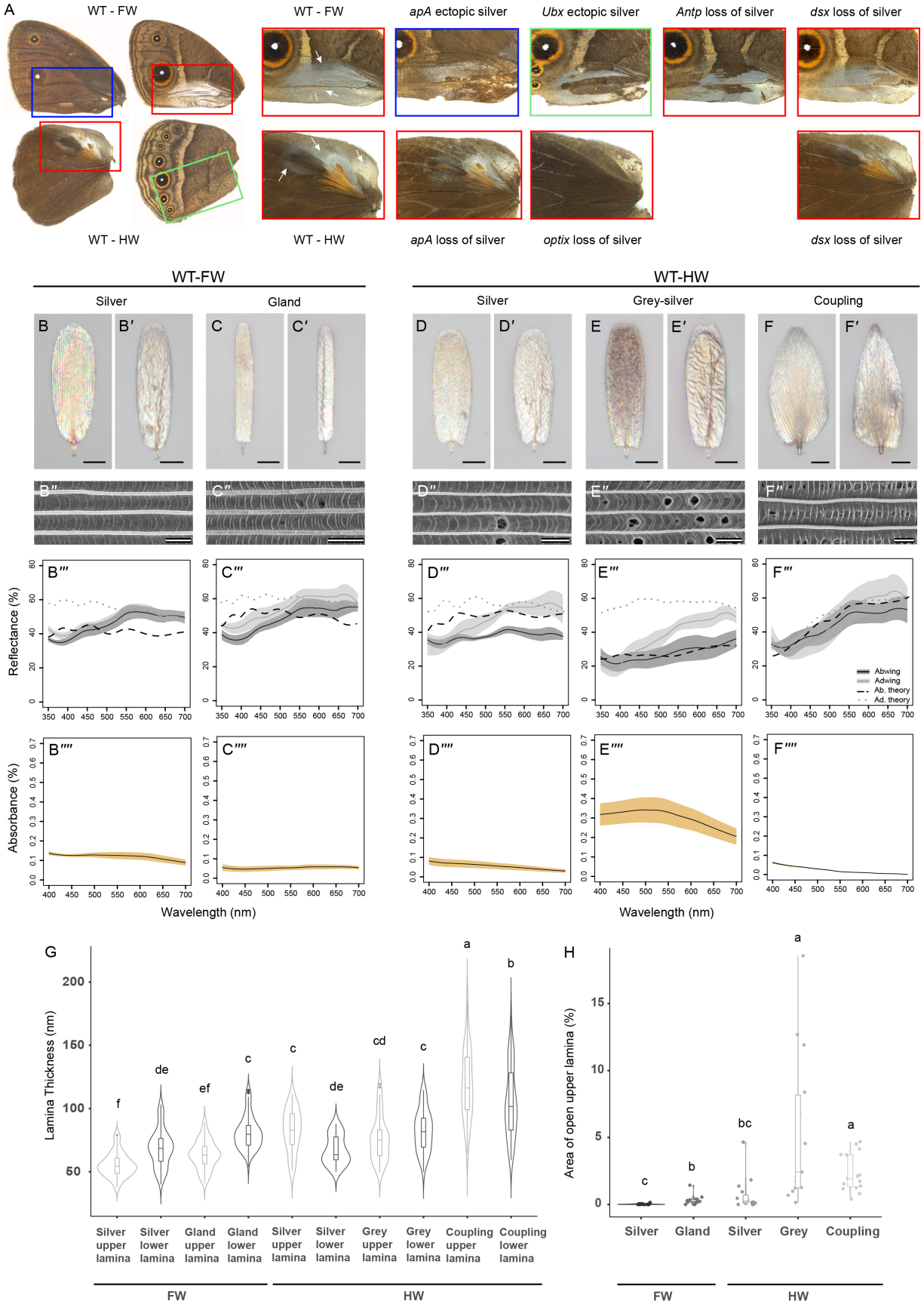
A
WT - FW
WT - FW
apA ectopic silver
Ubx ectopic silver
Antp loss of silver
dsx loss of silver
WT - HW
WT - HW
apA loss of silver
optix loss of silver
dsx loss of silver
WT-FW
WT-HW
Silver
Gland
Silver
Grey-silver
Coupling
Reflectance (%)
Absorbance (%)
Wavelength (nm)
Abwing
Adwing
Ab. theory
Ad. theory
G
Lamina Thickness (nm)
Silver upper lamina
Silver lower lamina
Gland upper lamina
Gland lower lamina
Silver upper lamina
Silver lower lamina
Grey upper lamina
Grey lower lamina
Coupling upper lamina
Coupling lower lamina
FW
HW
H
Area of open upper lamina (%)
Silver
Gland
Silver
Grey
Coupling
FW
HW

Figure 1: *B. anynana* crispants sampled in this study and broadband reflectors in wildtype *B. anynana*. (A) WT dorsal and ventral wing surfaces with magnified views of the silver scales alongside ectopic silver scales or silver to brown transformed scales in crispants of the five genes. The colored box outlines indicate the position on the different wing surfaces of the WT and crispant scales. White arrows in the WT panels indicate the five different silver scale types characterized. Optical microscopy images of the abwing (upperside) (B-F) and adwing (underside) (B′-F′) surfaces of single scales, SEM images of the abwing surface (B″-F″), measured and modeled reflectance (B‴-F‴) and absorbance spectra (B⁗-F⁗) of the WT forewing silver and gland scales and the hindwing silver, grey-silver and coupling scales respectively. (G) Violin plots of the upper and lower lamina thicknesses of the different forewing and hindwing silver scales. (H) Area of the open upper lamina of the different silver scales on the forewings and hindwings. Boxplots show the median, inner and outer quartiles and whiskers up to 1.5 times the inter-quartile range. Means sharing the same letter are not significantly different (Tukey-adjusted comparisons). Scale bars: B,B′-F,F′ are 20 μm and B″-F″ are 2 μm.

In order to theoretically model these broadband metallic colors, we measured the air gap, lower and upper lamina thicknesses from FIB-SEM cross-sections of the different silver scale types (Fig 1G, Supplementary Table S5 – source data). The mean upper and lower lamina thicknesses of the different metallic scale types ranged from approximately 55-120 nm, with the coupling scales having the thickest lower and upper laminas (Fig 1G). We modeled the theoretical adwing and abwing spectra, the latter by incorporating the measured absorptivity curves (Fig 1B⁗-F⁗), which produced broadband reflectance with a series of very shallow peaks, whose positions are largely consistent with those in the corresponding measured spectra (Fig 1B‴-F‴, Supp Fig S1). A lower lamina thin film of an appropriate thickness could, alone, produce a broadband silver color (Supp Fig S2A). However, our results indicated that the presence of the additional upper lamina enclosing an air gap with varying thickness increased the mean broadband reflectivity by around 11% (Supp Fig S2A). Furthermore, our hierarchical modeling (Supp Figs S2 and S3) suggests that the observed variation in the upper and lower lamina thicknesses cannot reproduce the relatively flat broadband reflectance even when the sclerotized ridges are included (Supp Figs S2A-C), whereas the variation in the air gap layer, alone, can sufficiently account for the broadband silvery

reflectance, including the patches of distinct colors (e.g. pink and green) seen in between ridges in high magnification light micrographs (Fig 1B,B′-F,F′, Supp Fig S2C) (24). Finally, our systematic parametric modeling (Supp Fig S3) revealed that the thicknesses of both upper and lower laminas for each of the silver scale types, except coupling, are more or less optimized to produce the maximum broadband reflectivity. By contrast, the air gap layer is sufficiently thick (> 750 nm) to ensure the broadband nature of the reflectivity, for a thickness of less than 500 nm will produce strong peak(s) with chromatic effects destroying the silvery appearance (Supp Fig S3). Interestingly, the modeling results predicted lower reflectivity at short wavelengths below 450 nm for the coupling scales (Supp Fig S2n) similar to their measured spectra (Fig 1F‴). Given that coupling scales are among the least pigmented (Fig. 1F⁗), our results indicate that this lower reflectivity is a previously undocumented structural rather than a pigmentary effect. Further corroborating these modeling results, a longitudinal cross-section of the coupling scale showed a decrease in the thickness of the lower lamina from base to tip (Supp Fig S4) and a concomitant change in the color of the scale from bronze/brown in the base/center to silver at the tips. This increased thickness near the base of the scale suppresses shorter wavelengths of light and leads to a greyish darker color (Fig 1F′), while optimum thickness towards the tip reinforces broadband silver reflectance.

Antp is a selector gene for rounded scale morphology and acts upstream of _dsx_ in the silver scale GRN

Both *Antp* and *dsx* male crispants exhibited a silver to brown color transformation on the forewing but had different effects on scale shape (Fig 2A-C). The rounded edges of the distal end of the silver scales of *Antp* crispants changed into serrated finger-like projections, similar to other brown scales on the same wing surface (Fig 2D, Supp Fig S5A). This was true in females also, where the normal rounded brown scales on the posterior region of the ventral forewings became brown scales with dentate margins in the crispants (Supp Fig S5B). In contrast, the loss of *dsx* expression in the same region produced brown scales with a rounded distal edge (Fig 2E). Furthermore, some of the *Antp* crispant brown scales exhibited unusual ridge and crossrib orientations near the distal tips of the scales, often lying perpendicular to the normal parallel arrangement of ridges (Fig 2F). In *Antp* male crispants, we also noticed small clonal patches of brown scales within the hindwing silver scale area (Fig 2G). Such clonal patches were also visible on female hindwings in homologous

193 regions of the wing, though not as contrasting (Supp Fig 5D). The brown scales in these clonal
194 patches had a dentate morphology similar to other dorsal hindwing scales, in contrast to the
195 rounded scales seen in the hindwing silver scale region in males or the homologous regions in
196 females (Supp Fig S5C, D).
197
198 Ultrastructure and pigmentation modifications accompanied the loss of silver reflectance in male
199 scales of both crispant types. The brown crispant scales had lower reflectivity in comparison with
200 the wildtype control scales (Fig 2A‴-C‴) and this was accompanied by an increase in absorbance
201 due to greater pigmentation (Fig 2A⁗-C⁗). The crispant brown scales also lost their continuous
202 upper lamina which now exhibited perforated windows (Fig 2A″-C″, I, Supplementary Tables
203 S1,2). Other ultrastructural modifications included an increase in lower lamina thickness (Fig 2H)
204 (Posthoc tests from LME, adjusted P-values <0.001; Supplementary Tables S3,4). *Antp* brown
205 scales had a greater lower lamina thickness (125.82 nm ± 19.7 nm) compared to the *dsx* brown
206 scales (91.9 nm ± 17.6nm) and both were significantly different from wildtype silver lower lamina
207 thickness (68.8 ± 14.75). The increase in pigmentation, loss of the upper lamina and increased
208 lower lamina thickness led to the loss of broadband metallic silver reflectance and created a brown
209 color due to the combination of pigments and the now dominant lower lamina reflectance (Fig
210 2A‴-C‴).
211
212 These results suggest that *Antp* is an upstream selector gene of silver scale color and morphology
213 in males and scale shape in females. *Antp* likely acts upstream of *dsx*, which appears to have similar
214 effects on color and upper lamina morphology but does not impact scale shape. To investigate the
215 extent to which Antp expression maps to silver scales, we examined the expression of Antp in 24-
216 hour male and female pupal wings. Antp protein was visible in punctate nuclei in the forewing
217 (Supp Fig S6A) and hindwing silver scale regions in males, especially around the future hindwing
218 gland (Supp Fig S6C), and also in female wings at homologous locations (Supp Fig S6B, D). Antp
219 protein expression was lower in the grey-silver scales on male hindwings (Supp Fig S6C). This
220 pattern on male hindwings was especially clear in a 48-hour pupal hindwing (Supp Fig S7). These
221 results indicate that Antp protein maps precisely to the area where silver scales develop on both
222 wings.
223

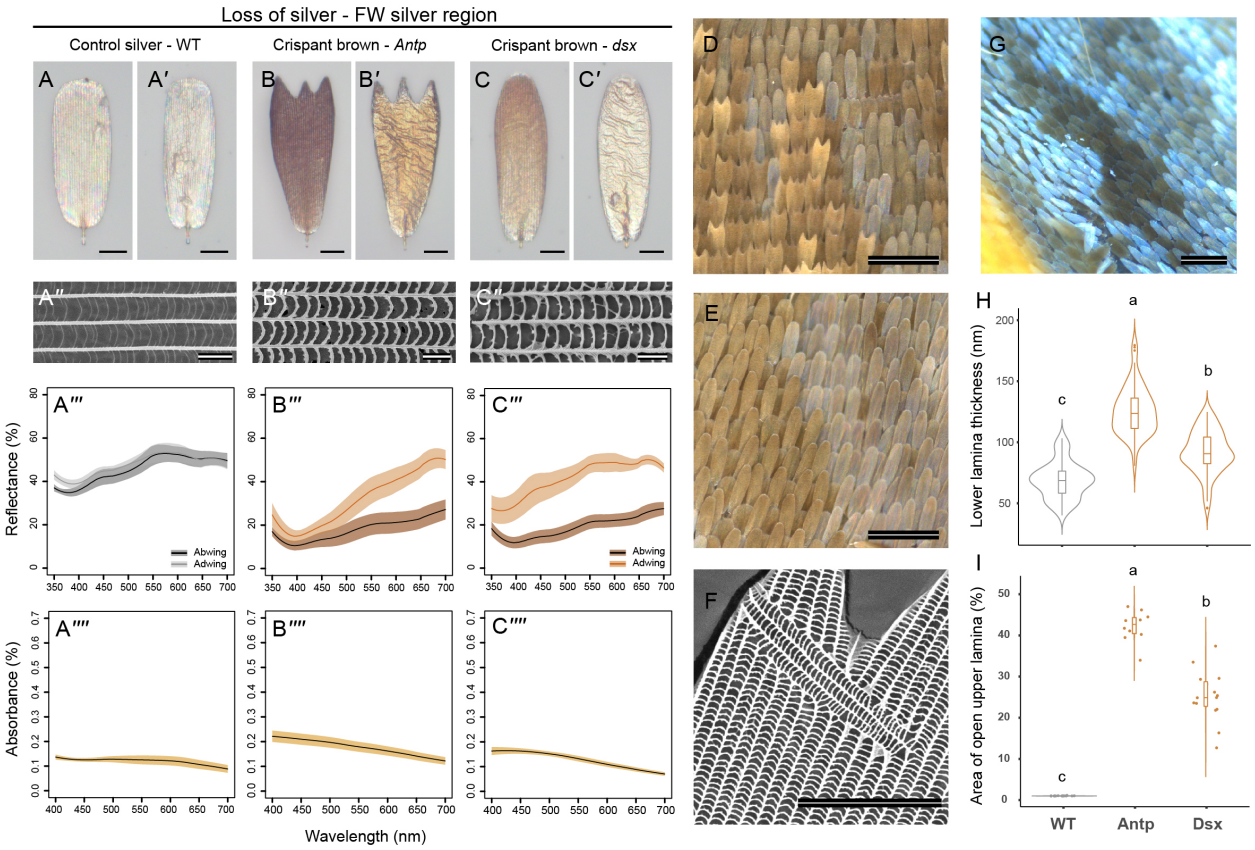

Figure 2: Characterization of the ultrastructure and pigmentation of the silver to brown scales in *Antp* and *dsx B. anynana* crispants. Optical microscopy images of the abwing (A-C) and adwing (A′-C′) surfaces, SEM images of the abwing surface (A″-C″), reflectance (A‴-C‴) and absorbance spectra (A⁗-C⁗) of the WT forewing control silver scales and the mutant brown scales of *Antp* and *dsx* crispants respectively. (D) Mosaic scale phenotype in *Antp* crispant forewing illustrating the mutant brown scales with dentate sculpting in the distal tips. (E) Mosaic scale phenotype in *dsx* crispant forewing illustrating the mutant brown scales with rounded distal tips. (F) SEM image of an *Antp* crispant forewing brown scale showing a nearly orthogonal ridge and crossrib orientation in the midst of the normal ridge and crossrib orientation parallel to the scale. These variations always occur at the distal tips of the crispant scales (N=4). (G) Mosaic scale phenotype in male *Antp* crispant hindwing illustrating the mutant brown scales with dentate sculpting in the distal tips. (H) Violin plots of the lower lamina thicknesses of the control silver scales and the crispant brown scales of *Antp* and *dsx* crispants (I) Total area of open upper lamina of the different control and mutant scales. Boxplots show the median, inner and outer quartiles and whiskers up to 1.5 times the inter-quartile range. Means sharing a letter are not significantly

240 different (Tukey-adjusted comparisons). Scale bars: A,A′-C,C′ and F are 20 µm, A″-C″ are 2 µm,
241 D, E,G are 200 µm.
242
243
244 **Ectopic silver scales gain an upper lamina, decrease the thickness of their lower lamina and**
245 **lose pigmentation**
246 We next investigated the ectopic forewing silver scales produced in the *apA* and *Ubx* crispants by
247 the transformation of non-reflective brown scales (Fig 1A). We characterized both ectopic silver
248 and gland scale types in *apA* crispants but only the ectopic silver scale type in the single *Ubx*
249 crispant due to size limitation of the mutant clone in that individual. Ectopic silver scales in both
250 *apA* and *Ubx* crispants looked similar to wildtype silver scales, including changes in cell shape
251 (Fig 3). The *Ubx* crispant scales exhibited an extensive transformation, from scalloped brown
252 scales to rounded silvery scales (Fig 3D, E), while the *apA* crispant scales changed primarily in
253 color and less extensively in shape (Fig 3A-C). The abwing and adwing surfaces of the ectopic
254 scales were metallic silvery thin films (Fig 3B, C, E). These scales were dramatically different
255 from the control brown scales from the same crispant regions which were brown in color from the
256 abwing side (Fig 3A, D) and had a bronze-golden adwing thin film (Fig 3A′, D′). Reflectance
257 spectra corresponded with the optical images, with the silver scales reflecting broadly (Fig 3A‴-
258 E‴). Ectopic metallic scales of both *apA* and *Ubx* crispants also lost pigmentation as compared to
259 the control brown scales, though there was variation between the different scale types (Fig 3A⁗-
260 E⁗).
261

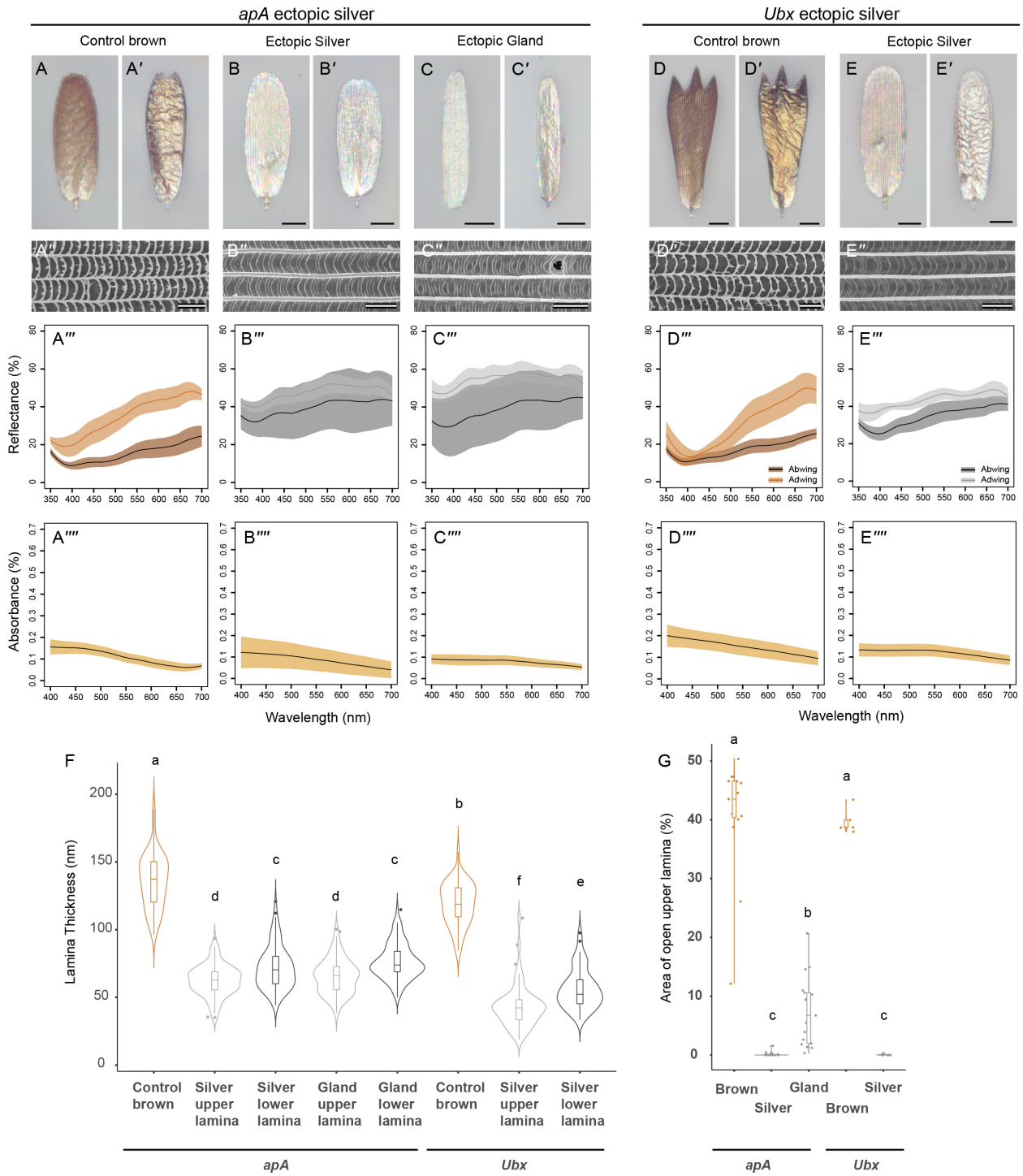

Figure 3: Characterization of ectopic silver scale ultrastructure and pigmentation in *apA* and *Ubx B. anynana* crispants. Optical microscopy images of the abwing (A-E) and adwing (A′-E′) surfaces, SEM images of the abwing surface (A″-E″), reflectance (A‴-E‴) and absorbance spectra (A⁗-E⁗) of the *apA* forewing control brown scales, ectopic silver and gland scales and the *Ubx* hindwing control brown scales and ectopic silver scales respectively. The control scales for these

crispants are from the same wings as the ectopic scales, close to the mosaic crispant patches. (F) Violin plots of the upper and lower lamina thickness of the control brown scales and the ectopic silver and gland scales of *apA* and *Ubx* crispants. (G) Area of open upper lamina of the different control and ectopic scales. Boxplots show the median, inner and outer quartiles and whiskers up to 1.5 times the inter-quartile range. Means sharing a letter are not significantly different (Tukey-adjusted comparisons). Scale bars: A,A′-E,E′ are 20 µm and A″-E″ are 2 µm.

Structural modifications accompanying brown to silver scale transformations, in *apA* and *Ubx* crispants, were opposite to those seen when silver scales became brown. Ectopic silver scales gained a closed upper lamina and an enclosed air layer, reduced their lower lamina thickness, and lost pigmentation in comparison to control brown scales (Fig 3A″-E″, F, G). The upper lamina transformation was complete for the *apA* and *Ubx* silver scale types, whereas many of the *apA* ectopic gland scales exhibited a partial transformation, having a significantly greater percentage of upper lamina open (Posthoc tests from LME, adjusted p-values <0.01; Supplementary Tables S1,2) (Fig 3G). All ectopic silver scale types exhibited a significant decrease in lower lamina thickness when compared to the control brown scales (Posthoc tests from LME: adjusted P-values <0.0001; Supplementary Tables S3,4). Similar to the wildtype forewing silver scales, the ectopic forewing silver scales in both *apA* and *Ubx* crispants also had thicker lower laminas as compared to the respective upper laminas (Supplementary Tables S3,4). The greater variability in the ultrastructural transformations and pigmentation of the *apA* ectopic silver scale types explains the greater variability in the abwing reflectance spectra measured from these crispant scales (Fig 3B‴, C‴).

apA, _dsx_ and _optix_ promote silver coloration via the gain of an upper lamina, decrease in lower lamina thickness and loss of pigmentation

On the hindwings, crispants of *apA*, *dsx*, and *optix* showed loss of metallic silver scales and transformation of these scales into brown scales. For *apA* these are the exact opposite phenotypes from those observed on the forewing, where *apA* transformed brown scales into ectopic silver scales. In *apA* and *dsx* crispants, hindwing silver and grey-silver scales were transformed into brown scales (Fig 4A-F) while in the *optix* crispants, the coupling silver scales became brown

scales (Fig 4G-H). Brown crispant scales of *apA* individuals exhibited a dentate morphology while those in *dsx* individuals exhibited some variation in morphology, from rounded scales in the silver region to sometimes dentate scales in the grey-silver region. Brown *optix* coupling scales displayed a noticeable change in morphology from the characteristic trowel-head shape of the control scales to an oblong morphology in the crispant brown scales (Fig 4G-H). Reflectance spectra reflected the change in coloration (Fig 4A‴ – H‴). In all instances of transformation, the adwing sides of the crispant scales were thin films reflecting a deep bronze-golden color instead of the silver to gold reflectance of the wildtype control scales (Fig 4A′-H′). In addition, in line with the silver to brown transformation, there was an increase in pigmentation in most scales (Fig 4A⁗-C⁗, G⁗-H⁗), except in the grey-silver region, where crispant brown scales, in both *apA* and *dsx* crispants, had decreased pigmentation as compared to the controls (Fig 4D⁗-F⁗), despite control scales displaying a lot of variation in pigmentation levels (Fig 4 D⁗).

Similar to the forewing silver to brown transformations, crispant brown scales on the hindwing, produced by all three genes, also exhibited a loss of the upper lamina (Fig 4A″-H″, J, Supplementary Tables S1,2). This was not a clean morphological change, with many scales exhibiting a gradualism in transformation, often having remnants of the lamina attached to the crossribs and ridges (Fig 4A″-H″, J). The lower lamina thickness of these scales also increased compared to wildtype silver controls (Posthoc tests from LME, adjusted P-values <0.001; Supplementary Tables S3,4). Both *apA* and *dsx* hindwing brown scales in the silver and grey-silver regions had significantly thicker lower laminas than control scales, while there was no change of lamina thickness in *optix* crispant brown scales (Fig 4I, Supplementary Tables S3,4).

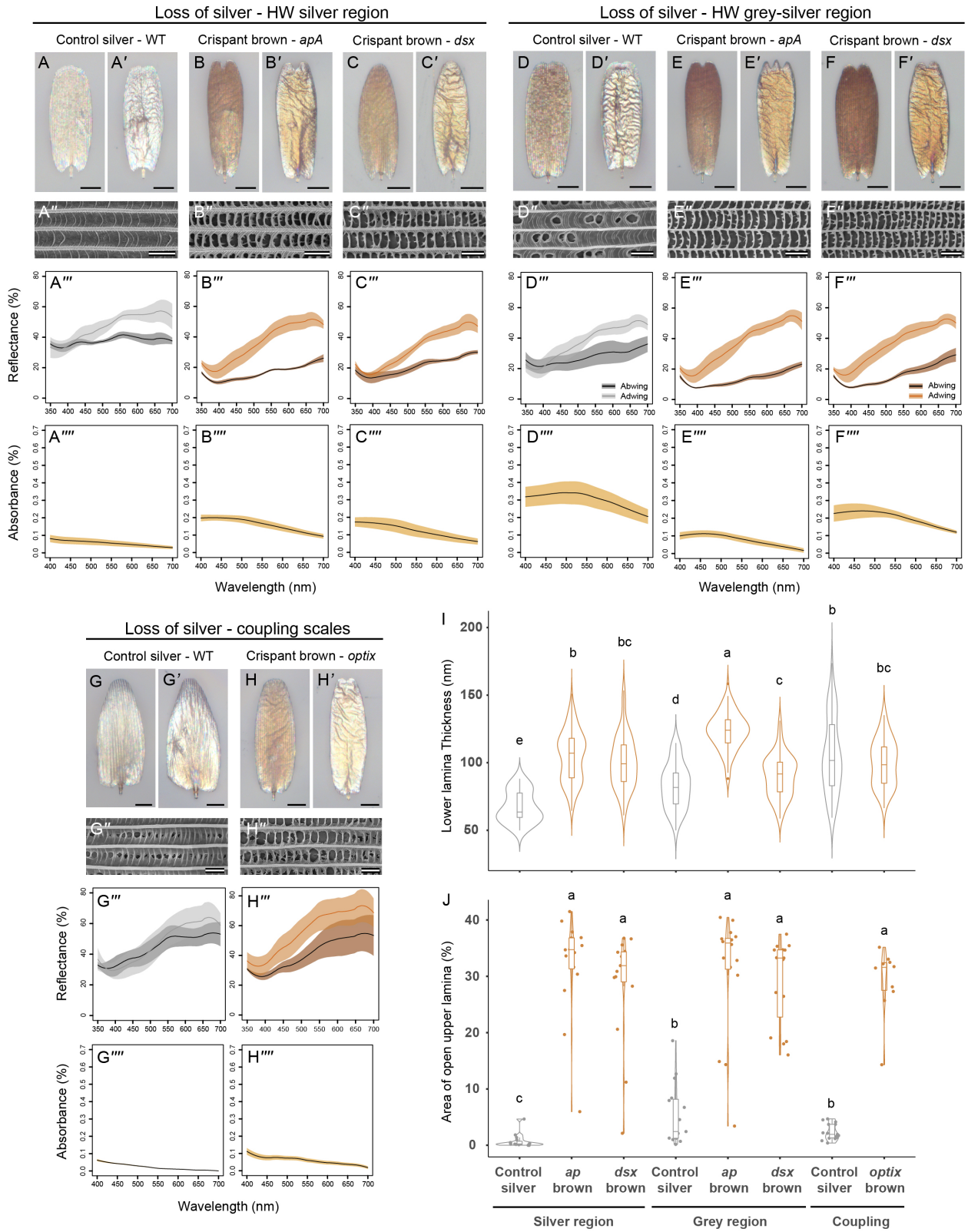

Figure 4: Characterization of the ultrastructure and pigmentation of transformed silver to brown scales in *apA*, *dsx* and *optix B. anynana* crispants. Optical microscopy images of the

abwing (A-H) and adwing (A'-H') surfaces, SEM images of the abwing surface (A″-H″), reflectance (A‴-H‴) and absorbance spectra (A⁗-H⁗) of the control WT silver scales and transformed crispant brown scales in the hindwing silver region (A-C), the hindwing grey-silver region (D-F) and the hindwing coupling scales (G-H). The control scales are WT silver scales from homologous regions on the wing. (I) Violin plots of the lower lamina thicknesses of control WT silver scales and the crispant brown scales of *apA, dsx* and *optix* crispants (G) Total area of open upper lamina of the different control and crispant brown scales. Boxplots show the median, inner and outer quartiles and whiskers up to 1.5 times the inter-quartile range. Means sharing a letter are not significantly different (Tukey-adjusted comparisons). Scale bars: A,A′-H,H′ are 20 µm and A″-H″ are 2 µm.

Discussion and conclusion

Metallic scales in *Bicyclus anynana* are undulatory broadband reflectors

We characterized five different metallic reflectors in *B. anynana* butterflies. Four out of the five scale types are present only in males, associated with the androconial regions that produce and secrete sex pheromones, while the fifth, the coupling scales, are found in both sexes near the base of the wings. All five metallic scale types investigated in this study produced broadband silver reflectance from an undulatory thin film achieved by the closure of the "open" windows present in typical wing scales. The sandwiched air gap layer of varying thickness between two chitinous laminas reflects spatially different wavelengths of light, resulting in a specular metallic color at the far-field due to additive color mixing. Such an ultrastructural modification involving the gain of a contiguous upper lamina leading to metallic coloration has been well-documented in multiple butterfly species across different families (21, 24), suggesting that the convergent evolution of metallic reflectors in butterflies can occur repeatedly with a few simple modifications to the basic scale architecture. Our modeling demonstrates that while butterflies can achieve broadband metallic colors by tuning just the lower lamina, the three-layer system comprising a sandwiched air layer between chitinous laminas is substantially brighter, perhaps explaining its repeated evolutionary origin (24). Moreover, the varying thickness of the air gap was the most important structural parameter to produce a nearly flat (smoothed out) broadband reflectance, while the upper and lower lamina thicknesses were more optimized for enhancing the broadband reflectivity. Pigmentation levels were low overall but varied among the different silver scales along with slight

359 variations in the total open area of the upper lamina. This intriguingly suggests that the amount of
360 pigmentation may be directly impacting the formation of the upper lamina, as previously
361 demonstrated in other scale types of *B. anynana* (33). We were unable to characterize the exact
362 pigment composition in these scales, but the absorbance spectra of the grey-silver scales suggests
363 that the pigments are not purely melanins but could instead be a combination of melanins and
364 additional pigments such as ommochromes (29).
365

366 **Each of five genes that led to gains and losses of metallic reflectance also changed**
367 **pigmentation levels and scale ultrastructure**

368 We discovered that disruptions to the five genes investigated (*Antp, dsx, apA, Ubx and optix*) lead
369 to simultaneous change in three scale features, suggestive of a switch-like or pleiotropic role for
370 these genes in determining the development of metallic scales. Transformation of metallic silver
371 scales into brown, non-reflecting scales in *Antp*, *dsx*, *apA* and *optix* crispants involved loss of an
372 upper lamina, gain in pigmentation levels, and an increase in lower lamina thickness. This was
373 generally true except in the case of the grey-silver scales of the hindwing where transformation to
374 brown scales led to a decrease in pigmentation. Likewise, gain of silver reflectance in scales of
375 *apA* and *Ubx* crispants was accompanied by the appearance of a continuous upper lamina that
376 closed the windows of the typical scale ground plan, a decrease in pigmentation levels, and a
377 decrease in the thickness of the lower lamina. The breadth of variation seen in individual crispant
378 brown scales and ectopic silver scales was potentially due to incomplete knockouts, and variation
379 in the protein function of each mutant allele. This was especially the case of *apA* crispants, possibly
380 due to the incomplete knockout of these genes in individual scales cells.
381

382 The gain and loss of an upper lamina with concurrent changes in the thickness of the lower lamina
383 suggests a possible conservation of total chitin production within a cell, but variable deposition
384 between the two laminas. There is some evidence for this in the forewing silver and gland scales
385 but not in the hindwing silver scale types. The summed thicknesses of the two laminas in the
386 wildtype forewing silver scales and ectopic silver scales was similar to the lower lamina thickness
387 of the forewing control brown scales and crispant brown scales. Though there is some indication
388 of the conservation of chitin production within a single cell, testing this proposition in the future
389 will require finer measurements of chitin production within different scale color types. Further,

390 Matsuoka and Monteiro (33) speculated that downstream effector genes such as *yellow* could affect
391 cuticle polymerization around crossribs to create windows because *yellow B. anynana* crispant
392 black and brown scales exhibited an upper lamina covering the windows. Given the low amounts
393 of pigmentation seen in the different silver scale types, it is possible that the gene *yellow* is not
394 highly expressed in silver scales, mirroring *yellow* crispant scales. *yellow* would then be a potential
395 downstream target, that would be repressed by the silver scale GRN. This hypothesis could be
396 tested by measuring levels of *yellow* expression in the different colored vs silver scales of *B.*
397 *anynana*, as well as in crispant individuals during development.
398

399 ***Antp* is a selector gene for rounded scales and acts through DsxM to determine silver scales**

400 Investigation of the mutant brown scales in *Antp* crispants uncovered an important role for this
401 gene in determining a rounded scale morphology. Scales on the posterior ventral forewing and
402 anterior dorsal hindwing of both sexes of *B. anynana*, a region where Antp is strongly expressed
403 (Supp Fig S6), normally have rounded distal ends, appearing silver in males and shades of brown
404 in females. In *Antp* crispants, the rounded scales developed serrated distal tips in both sexes,
405 concurrent with the transformation of silver to brown color in males only. These crispant brown
406 scales with serrated edges were similar to the scales usually found on the rest of the ventral
407 forewing (Supp Fig S5A, B) or dorsal hindwing (Supp Fig S5C, D), indicating that *Antp* is essential
408 for converting a serrated distal scale edge into a rounded scale. Furthermore, this result suggests
409 that *Antp* acts upstream of *dsx* in the forewing and hindwing silver scale GRN because male *dsx*
410 crispants exhibited a more restricted silver to brown transformation, still displaying the rounded
411 distal edge of a typical silver scale, instead of the dentate morphology. We propose that the protein
412 Antp activates *dsx* in the posterior ventral forewing or anterior dorsal hindwing (Fig 5). In females,
413 Antp would lead to the production of the DsxF protein splice variant, resulting in brown scales
414 with a rounded morphology since DsxF has no function in silver scale development (34). In males,
415 *Antp* would activate DsxM protein splice variant, which leads to the development of rounded silver
416 scales in both regions (34). Interestingly, the metallic silver scales on male forewing and hindwings
417 fall into two populations with different aspect ratios: the shorter silver scales covering most of the
418 region and the longer, thin gland scales that cover only the underlying pheromone glands (38).
419 The spatially defined occurrence of the long, thin gland scales is likely specified by the spatially
420 restricted expression of some unknown gland-specific gene, downstream of DsxM in the silver

scale GRN.

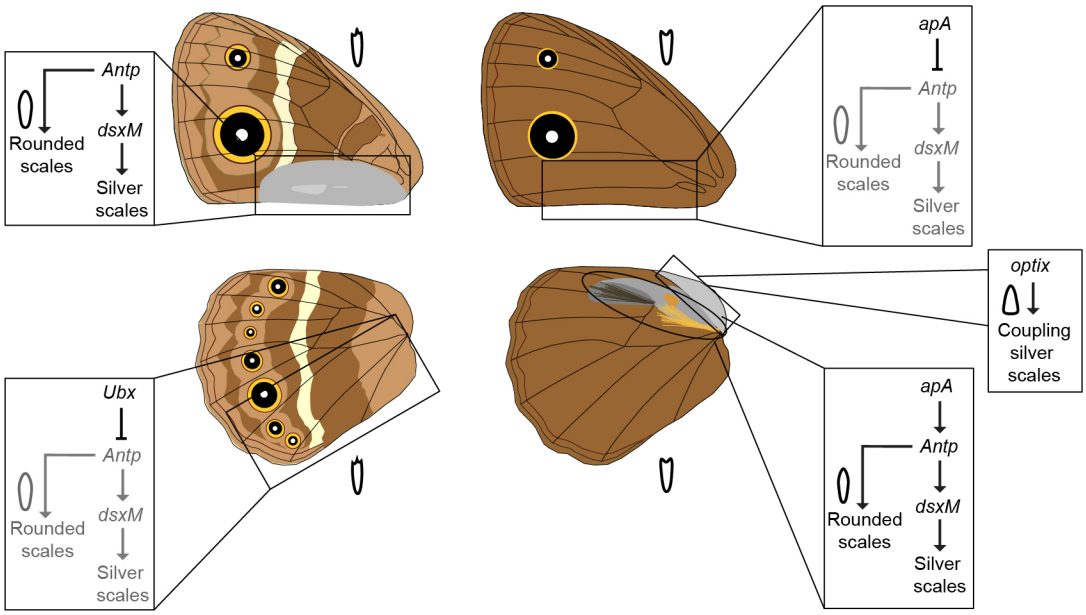

Figure 5: Proposed gene regulatory network (GRN) controlling silver scale development and scale shape in different wing regions of a male *B. anynana*. For each wing region, GRNs are indicated within boxes. The scale schematics inside the boxes represent the scale shape when the 'rounded scales' part of the network is active (dark lines). Repressed parts of the network are in grey. The scale schematics outside the boxes, next to each wing surface, reflect the scale shape generally found on that surface otherwise.

The unusual ridge and crossrib orientation, almost orthogonal to the normal orientation, seen in a few *Antp* crispant brown scales, hinted at a role for this gene in ridge patterning during the early stages of scale development. In developing scales, the positioning and orientation of ridges is determined by the spacing of F-actin filaments that emanate from the base of the scale, parallel to the scale's long axis (39, 40). The disrupted and abrupt change in orientation of the ridges and their corresponding crossribs in the *Antp* crispant scales suggests a potential disruption of the orientation of F-actin filaments. Based on the distal domain of occurrence of the unusual ridge patterns, along with the rounded to serrated distal edge change seen in *Antp* crispants, we speculate that *Antp* regulates the distal expression of an unknown factor, possibly a cytoskeletal component, that determines scale morphology and ridge/crossrib orientation. Hox genes such as *Abd-B* have

been identified to activate cytoskeletal components like cadherins in the development of posterior spiracles of *Drosophila* (41). Furthermore, *Ubx* directly regulates cytoskeletal components such as actin and contributes to cytoskeletal reorganization in haltere cells (42). In that context, our results identify a novel post-embryonic role of a Hox gene in the determination of the shape of a single cell. How *Antp* directs scale shape and ridge orientation, and which genes are its downstream targets, remains an exciting avenue for future work.

The silver scale GRN is modulated in various ways across the fore- and hindwings

The appearance of forewing silver and gland scales in ectopic dorsal locations on the forewings of *apA* crispants and ventral locations on the hindwings of *Ubx* crispants, lead us to propose that both genes are repressing the forewing silver scale GRN (Fig 5). *Ubx* is a well-known homeotic gene whose expression is restricted to the hindwings of many insects and which functions in determining hindwing shape and color patterns in butterflies (36, 43–45). Knockout of *Ubx* in *B. anynana* converts hindwing patterns into forewing patterns (36). Since *Antp* is a top regulator of the silver scale GRN, these results suggest that *Ubx* represses *Antp* expression on the ventral hindwings. Recent work showed that upon loss of *Ubx*, *Antp* is strongly expressed on the hindwings (Matsuoka and Monteiro, in prep). We propose that the silver scales observed on the ventral hindwing of the *Ubx* male crispant resulted from the de-repression of *Antp* in that region, followed by the activation of DsxM, and the development of rounded silver scales typical of the ventral forewing (Fig 5). Along similar lines, *apA* is a dorsal surface-specific gene and in *apA* crispants, forewing ventral silver and gland scales appeared on the dorsal forewing surface (35). This is again suggestive of *apA* repressing *Antp* on the dorsal forewing surface. Upon de-repression, Antp activates DsxM and this leads to the development of the metallic silver scales on the dorsal surface of males (Fig 5). This regulatory circuit appears to be different from the development of somatic mesodermal muscle tissues in *Drosophila* where *Antp* directly and positively regulates *apterous* (46). Our proposed forewing silver scale GRN thus identifies *Antp* as a top regulator, directing metallic scale development via *dsx*. *apA* and *Ubx* are repressors of this network on the dorsal forewings and ventral hindwings, respectively (Fig 5). However, the molecular basis of the direct or indirect regulatory interactions between these different genes remains to be identified.

473 On the hindwings, the silver and grey-silver scale GRN retains the same topology, with *Antp*
474 determining a rounded scale shape and acting via *dsx* to determine silver scale development (Fig
475 5). In contrast to its repressive role on the dorsal forewing silver scale GRN, *apA* acts as an
476 activator of the GRN on the hindwings. The difference in levels of Antp protein expression
477 between the silver and grey-silver scale regions suggests that varying thresholds of this protein are
478 functionally relevant in the two scale types. Lastly, *optix* is necessary to create a silver coupling
479 scale but it also modulates scale shape from an oblong to a trowel-shaped morphology. Its
480 expression in coupling scales of other butterflies such as *Heliconius* implicates a conserved role
481 for *optix* in the development of trowel-shaped coupling scales (47, 48).
482
483 In conclusion, this study identified the structural and photonic origin of broadband silver coloration
484 by comparing silver scales in WT and crispants for five genes in the butterfly *B. anynana*. Based
485 on the epistasis between the investigated genes, we proposed a GRN for metallic scale
486 development in butterflies. We identified *Antp* as an important top-level gene in the regulatory
487 network for silver scale development and a novel role for this Hox gene in determining the shape
488 of single cells.
489

490 **Materials and methods**

491 Crispant individuals and sampled scale types

492 All crispant individuals used in this study were previously generated in our lab by CRISPR Cas9-
493 mediated gene editing in *B. anynana. B. anynana* crispants were for the following genes: *apterous*
494 *A* (*apA*) (35), *Ultrabithorax* (*Ubx*) (36), *doublesex* (*dsx*) (34), *Antennapedia* (*Antp*) (36) and *optix*
495 (37). Five different silver scale types were sampled, namely, the silver and the gland scales on the
496 androconial patch of male ventral forewings, the silver and grey-silver scales near the androconial
497 patches of male dorsal hindwings and the coupling scales near the base of the dorsal hindwing in
498 females (Fig 1A).
499

500 Scanning electron microscopy

501 Five to six scales from different regions of the crispant individuals (Fig 1A) were individually
502 mounted onto carbon tape and sputter coated with gold using a JFC-1100 Fine Coat Ion Sputter
503 (JEOL Ltd. Japan). Images were obtained using a JEOL JSM-6510LV scanning electron

504 microscope (JEOL Ltd. Japan). For the wildtype, *apA* and *dsx* crispants, three different individuals
505 were sampled for each case. Two individuals were sampled for *Antp* and *optix* crispants while only
506 one crispant was obtained for *Ubx.*
507
508 Percentage area of open upper lamina measurements
509 From the SEM images, the percentage of area of open upper lamina was calculated using ImageJ
510 1.52a (Java 1.8.0_112) (49). A 20 μm^2 (10 μm^2 for gland scales) region of interest was defined
511 approximately at the center of the scale and the region outside cleared. A thresholding was applied
512 based on the values of the bright (ridge and crossribs) and dark (windows) regions of the SEM.
513 The dark areas were selected and added to the ROI Manager in ImageJ using the Analyze Particles
514 function. The selected regions were combined using the OR function in the ROI Manager. The
515 combined area of the open upper lamina within the defined regions was measured and converted
516 into a percentage.
517
518 Focused ion beam scanning electron microscopy (FIB-SEM)
519 FIB-SEM was used to measure the lower lamina, upper lamina, and air gap thicknesses for all
520 scale types in our analysis and corrected for tilted perspective (measured thickness / sin 52°).
521 Briefly, samples were prepared by sputter-coating with platinum to increase conductivity. The
522 scales were milled using a gallium ion beam on a FEI Versa 3D with the following settings: beam
523 voltage −8kV, beam current −12pA at a 52° tilt. Image acquisition was performed in the same
524 equipment with the following settings: beam voltage −5kV, beam current −13pA. Milling was
525 done at the center of each scale. Thickness measurements were done in ImageJ. For each scale
526 type, ten measurements were taken per scale with 3-16 scales sampled from 1-2 individuals.
527 Measurements were made along most of the lower lamina which is uniform, excluding the region
528 around the ridge base, where the thickness is highly variable.
529
530 Optical imaging and UV-VIS-NIR microspectrophotometry
531 Light microscope images of individual scales were recorded using the 20X lens of a uSight-2000-
532 Ni microspectrophotometer (Technospex Pte. Ltd., Singapore) and a Touptek U3CMOS-05
533 camera. Scales were individually mounted on a glass slide or in a refractive index matching
534 medium (clove oil) and multiple images at different focal planes (z-stack) were obtained. Stacking

was done in Adobe Photoshop v 22.5.1 (Adobe, California, USA).

Normal-incidence UV-VIS-NIR reflectance spectra of scales were acquired using the same microspectrophotometer setup but with a 100x objective. Spectra with usable range between 335-950 nm were collected using a high NA 100x objective from a ~2 µm sized spot (100 ms integration time, 10x averaging) and calibrated using an Avantes WS-2 reference tile made of white diffuse polytetrafluoroethylene. Individual scales were mounted on a black carbon tape and illuminated with a Mercury-Xenon lamp (ThorLabs Inc., New Jersey, USA). Measurements were taken from both abwing and adwing surfaces. For each scale type, measurements from five to ten individual scales from one individual were averaged. Absorbance spectrum was measured for individual scales immersed in a refractive index matching liquid (clove oil) using a 20X objective. Six to eight individual measures from one individual were averaged for each crispant type and wildtype. Analysis and spectral plots were done in R Studio 1.4.1106 with R 4.0.4 (50) using the R-package *pavo* (v 2.7) (51).

Acknowledgements

We thank Tirtha Das Banerjee for providing us the *optix* crispants, Yuji Matsuoka for providing us the *Antp* and *Ubx* crispants and Emilie Dion for helpful discussions on the statistics. We thank Sree Vaishnavi Sundararajan and Gianluca Grenci (MBI) for access and help with SEM, and the Pennycook group (MSE) for use of FIB-SEM. This research was supported by the National Research Foundation (NRF) Singapore under the Competitive Research Programme (NRF-CRP20-2017-0001 Award) and the National University of Singapore.

Author Contributions

A.P and A.M conceived and designed the study. A.P, C.F and V.S collected the spectral measurements. A.P and C.F collected the SEM data and C.F collected the FIB-SEM data. V.S performed the theoretical modeling. A.P analyzed all the data and did all the immunostainings. A.P wrote the manuscript with inputs from all the authors.

References

1. M. F. Land, The physics and biology of animal reflectors. *Prog. Biophys. Mol. Biol.* **24**,

75–106 (1972).

2. A. E. Seago, P. Brady, J.-P. Vigneron, T. D. Schultz, Gold bugs and beyond: A review of iridescence and structural colour mechanisms in beetles (Coleoptera). *J. R. Soc. Interface* **6 Suppl 2**, S165–S184 (2009).

3. A. C. Neville, Metallic gold and silver colours in some insect cuticles. *J. Insect Physiol.* **23**, 1267–1274 (1977).

4. E. J. Denton, M. F. Land, Mechanism of reflexion in silvery layers of fish and cephalopods. *Proc. R. Soc. London. Ser. B, Biol. Sci.* **178**, 43–61 (1971).

5. A. L. Holt, A. M. Sweeney, S. Johnsen, D. E. Morse, A highly distributed Bragg stack with unique geometry provides effective camouflage for Loliginid squid eyes. *J. R. Soc. Interface* **8**, 1386–1399 (2011).

6. D. Gur, *et al.*, The Dual Functional Reflecting Iris of the Zebrafish. *Adv. Sci.* **5**, 1800338 (2018).

7. E. J. Denton, Review lecture: on the organization of reflecting surfaces in some marine animals. *Philos. Trans. R. Soc. London. Ser. B, Biol. Sci.* **258**, 285–313 (1970).

8. S. Johnsen, Hide and Seek in the Open Sea: Pelagic Camouflage and Visual Countermeasures. *Ann. Rev. Mar. Sci.* **6**, 369–392 (2014).

9. H.-J. Wagner, R. H. Douglas, T. M. Frank, N. W. Roberts, J. C. Partridge, A Novel Vertebrate Eye Using Both Refractive and Reflective Optics. *Curr. Biol.* **19**, 108–114 (2009).

10. B. D. Wilts, P. Pirih, K. Arikawa, D. G. Stavenga, Shiny wing scales cause spec(tac)ular camouflage of the angled sunbeam butterfly, Curetis acuta. *Biol. J. Linn. Soc.* **109**, 279–289 (2013).

11. D. G. Stavenga, H. L. Leertouwer, D. C. Osorio, B. D. Wilts, High refractive index of melanin in shiny occipital feathers of a bird of paradise. *Light Sci. Appl.* **4**, e243–e243 (2015).

12. S. N. Nan, *et al.*, Keeping cool: Enhanced optical reflection and radiative heat dissipation in Saharan silver ants. *Science (80-.).* **349**, 298–301 (2015).

13. P. Vukusic, J. R. Sambles, Photonic structures in biology. *Nature* **424**, 852–5 (2003).

14. S. Kinoshita, S. Yoshioka, J. Miyazaki, Physics of structural colors. *Reports Prog. Phys.* **71** (2008).

15. M. Srinivasarao, Nano-Optics in the Biological World: Beetles, Butterflies, Birds, and Moths. *Chem. Rev.* **99**, 1935–1962 (1999).
16. a R. Parker, D. R. McKenzie, M. C. J. Large, Multilayer reflectors in animals using green and gold beetles as contrasting examples. *J. Exp. Biol.* **201**, 1307–1313 (1998).
17. E. D. Finlayson, L. T. McDonald, P. Vukusic, Optically ambidextrous circularly polarized reflection from the chiral cuticle of the scarab beetle Chrysina resplendens. *J. R. Soc. Interface* **14** (2017).
18. R. A. Steinbrecht, Fine structure and development of the silver and golden cuticle in butterfly pupae. *Tissue Cell* **17**, 745–762 (1985).
19. R. a. Steinbrecht, W. Mohren, H. K. Pulker, D. Schneider, Cuticular Interference Reflectors in the Golden Pupae of Danaine Butterflies. *Proc. R. Soc. B Biol. Sci.* **226**, 367–390 (1985).
20. D. R. McKenzie, Y. Yin, W. D. McFall, Silvery fish skin as an example of a chaotic reflector. *Proc. R. Soc. London. Ser. A Math. Phys. Sci.* **451**, 579–584 (1995).
21. P. Vukusic, R. Kelly, I. Hooper, A biological sub-micron thickness optical broadband reflector characterized using both light and microwaves. *J. R. Soc. Interface* **6 Suppl 2**, S193-201 (2009).
22. C. Kilchoer, U. Steiner, B. D. Wilts, Thin-film structural coloration from simple fused scales in moths. *Interface Focus* **9** (2019).
23. L. D'Alba, B. Wang, B. Vanthournout, M. D. Shawkey, The golden age of arthropods: Ancient mechanisms of colour production in body scales. *J. R. Soc. Interface* **16** (2019).
24. A. Ren, *et al.*, Convergent Evolution of Broadband Reflectors Underlies Metallic Coloration in Butterflies . *Front. Ecol. Evol.* **8**, 206 (2020).
25. A. Dolinko, *et al.*, Analysis of the optical properties of the silvery spots on the wings of the Gulf Fritillary, Dione vanillae. *Sci. Rep.* **11**, 19341 (2021).
26. T. J. Simonsen, Comparative morphology and evolutionary aspects of the reflective under wing scale-pattern in Fritillary butterflies (Nymphalidae: Argynnini). *Zool. Anz.* **246**, 1–10 (2007).
27. Z. Qingqing, *et al.*, Fossil scales illuminate the early evolution of lepidopterans and structural colors. *Sci. Adv.* **4**, e1700988 (2021).
28. B. Vanthournout, *et al.*, Springtail coloration at a finer scale: mechanisms behind vibrant

628 collembolan metallic colours. *J. R. Soc. Interface* **18**, 20210188 (2021).
629 29. B. R. Wasik, *et al.*, Artificial selection for structural color on butterfly wings and
630 comparison with natural evolution. *Proc. Natl. Acad. Sci.* (2014)
631 https:/doi.org/10.1073/pnas.1402770111 (August 5, 2014).
632 30. R. C. Thayer, F. I. Allen, N. H. Patel, Structural color in Junonia butterflies evolves by
633 tuning scale lamina thickness. *Elife* **9**, e52187 (2020).
634 31. R. H. Siddique, S. Vignolini, C. Bartels, I. Wacker, H. Hölscher, Colour formation on the
635 wings of the butterfly Hypolimnas salmacis by scale stacking. *Sci. Rep.* **6**, 36204 (2016).
636 32. L. Livraghi, *et al.*, Cortex cis-regulatory switches establish scale colour identity and
637 pattern diversity in heliconius. *Elife* **10**, 1–31 (2021).
638 33. Y. Matsuoka, A. Monteiro, Melanin Pathway Genes Regulate Color and Morphology of
639 Butterfly Wing Scales. *Cell Rep.* **24**, 56–65 (2018).
640 34. A. Prakash, A. Monteiro, Doublesex Mediates the Development of Sex-Specific
641 Pheromone Organs in Bicyclus Butterflies via Multiple Mechanisms. *Mol. Biol. Evol.* **37**,
642 1694–1707 (2020).
643 35. A. Prakash, A. Monteiro, *apterous A* specifies dorsal wing patterns and sexual traits in
644 butterflies. *Proc. R. Soc. B Biol. Sci.* (2018) https:/doi.org/10.1098/rspb.2017.2685.
645 36. Y. Matsuoka, A. Monteiro, Hox genes are essential for the development of eyespots in
646 Bicyclus anynana butterflies. *Genetics* **217** (2021).
647 37. T. Das Banerjee, S. K. Shan, A. Monteiro, optix is involved in
648 eyespot development via a possible positional information mechanism. *bioRxiv*,
649 2021.05.22.445259 (2021).
650 38. E. Dion, A. Monteiro, J. Y. Yew, Phenotypic plasticity in sex pheromone production in
651 Bicyclus anynana butterflies. *Sci. Rep.* **6**, 1–13 (2016).
652 39. A. Dinwiddie, *et al.*, Dynamics of F-actin prefigure the structure of butterfly wing scales.
653 *Dev. Biol.* **392**, 404–418 (2014).
654 40. C. R. Day, J. J. Hanly, A. Ren, A. Martin, Sub-micrometer insights into the cytoskeletal
655 dynamics and ultrastructural diversity of butterfly wing scales. *Dev. Dyn.* **248**, 657–670
656 (2019).
657 41. B. Lovegrove, *et al.*, Coordinated Control of Cell Adhesion, Polarity, and Cytoskeleton
658 Underlies Hox-Induced Organogenesis in Drosophila. *Curr. Biol.* **16**, 2206–2216 (2006).

42. A. Pavlopoulos, M. Akam, Hox gene Ultrabithorax regulates distinct sets of target genes at successive stages of Drosophila haltere morphogenesis. *Proc. Natl. Acad. Sci.* **108**, 2855–2860 (2011).
43. X. Tong, S. Hrycaj, O. Podlaha, A. Popadic, A. Monteiro, Over-expression of Ultrabithorax alters embryonic body plan and wing patterns in the butter fl y Bicyclus anynana. *Dev. Biol.* **394**, 357–366 (2014).
44. Y. Tomoyasu, S. R. Wheeler, R. E. Denell, Ultrabithorax is required for membranous wing identity in the beetle Tribolium castaneum. *Nature* **433**, 643–647 (2005).
45. S. D. Weatherbee, *et al.*, Ultrabithorax function in butterfly wings and the evolution of insect wing patterns. *Curr. Biol.* **9**, 109–115 (1999).
46. M. Capovilla, Z. Kambris, J. Botas, Direct regulation of the muscle-identity gene apterous by a Hox protein in the somatic mesoderm. *Development* **128**, 1221–1230 (2001).
47. A. Martin, *et al.*, Multiple recent co-options of Optix associated with novel traits in adaptive butterfly wing radiations. *Evodevo* **5**, 1–13 (2014).
48. L. Zhang, A. Mazo-Vargas, R. D. Reed, Single master regulatory gene coordinates the evolution and development of butterfly color and iridescence. *Proc. Natl. Acad. Sci.* **114**, 10707 LP – 10712 (2017).
49. C. A. Schneider, W. S. Rasband, K. W. Eliceiri, NIH Image to ImageJ: 25 years of image analysis. *Nat. Methods* **9**, 671–675 (2012).
50. R Core Team, R: A Language and Environment for Statistical Computing (2021).
51. R. Maia, H. Gruson, J. A. Endler, T. E. White, pavo 2: New tools for the spectral and spatial analysis of colour in r. *Methods Ecol. Evol.* **10**, 1097–1107 (2019).